

# Planar-integrated magneto-optical trap

Liang Chen,<sup>1,4</sup> Chang-Jiang Huang,<sup>1,4</sup> Xin-Biao Xu,<sup>1,4</sup> Zheng-Tian Lu,<sup>2,4</sup>  
 Zhu-Bo Wang,<sup>1,4</sup> Guang-Jie Chen,<sup>1,4</sup> Ji-Zhe Zhang,<sup>1,4</sup> Hong X. Tang,<sup>3</sup> Chun-Hua Dong,<sup>1,4</sup>  
 Wen Liu,<sup>5</sup> Guo-Yong Xiang,<sup>1,4</sup> Guang-Can Guo,<sup>1,4</sup> and Chang-Ling Zou<sup>1,4,\*</sup>

<sup>1</sup>Key Laboratory of Quantum Information, Chinese Academy of Sciences,  
 University of Science and Technology of China, Hefei 230026, P. R. China.

<sup>2</sup>Hefei National Laboratory for Physical Sciences at the Microscale,  
 University of Science and Technology of China, Hefei, Anhui, China, 230026

<sup>3</sup>Department of Electrical Engineering, Yale University, New Haven, CT 06511, USA

<sup>4</sup>CAS Center For Excellence in Quantum Information and Quantum Physics,  
 University of Science and Technology of China, Hefei, Anhui 230026, P. R. China.

<sup>5</sup>USTC Center for Micro-and Nanoscale Research and Fabrication,  
 University of Science and Technology of China, Hefei, Anhui 230026, P. R. China.

(Dated: July 16, 2021)

The magneto-optical trap (MOT) is an essential tool for collecting and preparing cold atoms with a wide range of applications. We demonstrate a planar-integrated MOT by combining an optical grating chip with a magnetic coil chip. The flat grating chip simplifies the conventional six-beam configuration down to a single laser beam; the flat coil chip replaces the conventional anti-Helmholtz coils of a cylindrical geometry. We trap  $10^4$  cold  $^{87}\text{Rb}$  atoms in the planar-integrated MOT, at a point 3 – 9 mm above the chip surface. This novel configuration effectively reduces the volume, weight, and complexity of the MOT, bringing benefits to applications including gravimeter, clock and quantum memory devices.

## I. INTRODUCTION

The magneto-optical trap (MOT) is one of the most important experimental platforms in atomic physics [1–4]. Cold atoms prepared by a MOT are widely used in quantum measurement and metrology applications [5–7]. For example, the atomic gravimetry with precision achieving  $\mu\text{Gal}/\sqrt{\text{Hz}}$  has been demonstrated [8]. The conventional MOT apparatus consists of three orthogonal pairs of retro-reflected laser beams and a pair of anti-Helmholtz coils in a cylindrical geometry [9].

Over the past decade, great efforts have been devoted to minimizing the MOT system. Most attentions are paid to reducing the bulky optical system. For example, by using a pyramidal retroreflector, only one incident laser beam is needed [10–13]. More recently, the idea was further developed by replacing the pyramidal retroreflector with a completely flat chip consisting of three gratings, demonstrating a MOT that can capture as many as  $10^7$  atoms with a single incident laser beam [14–18]. In contrast, the original bulky anti-Helmholtz coils still remain. Although U- or Z-shaped external Helmholtz coils were employed in an atom chip to assist the MOT, external Helmholtz coils were still required to provide a bias field [12, 13, 19–22].

In this work, we develop a planar-integrated MOT (piMOT) configuration based on both a grating chip and a planar  $3\text{cm} \times 3\text{cm}$  coil chip. The coil chip generates a quadrupole magnetic field several millimeters above the chip surface, matching the working points of the optical grating chip. While carrying a current of 0.9 A, the magnetic field gradient reaches 9.8 G/cm, and the low working voltage of 2.5 V and power of 2.5 W allows it to be powered by batteries. With both chips stacked outside a glass vacuum cell, we trap  $10^4$   $^{87}\text{Rb}$

atoms. The piMOT is simple, portable, and low-cost. It opens the possibility for further monolithic integration of the cold atom system with photonic chips [23–26], with future applications including portable gravimeter [27–30], clock [31–35] and quantum memory devices [36–39].

## II. THE COIL CHIP

The atoms are trapped in the MOT at the working point where the field equals zero and strong field gradients are present in all directions [40]. A conventional MOT generates this magnetic field using a pair of anti-Helmholtz coils [9], which is composed by a pair of identical coils (same radius  $R$ , current  $I$ , and turns  $N$ ) with opposite current directions, as shown in Fig. 1(a). The working point of this coil configuration is exactly its geometrical center. This cylindrical geometry poses limitations on a compact cold-atom system. For example, the vacuum cell needs to be inserted in between the pair of coils, thus limiting the minimum size of the coils. In order to reach the required  $\sim 10$  G/cm field gradient, the required currents in the coils grow with the cube of the coil size, which then leads to heat dissipation problems. These limitations can be overcome with a planar coil design to achieve a compact system.

We propose the coplanar annular coil chip [Fig. 1(b)], consisting of two coaxial coils with different radii  $R_1$  and  $R_2$  ( $R_1 < R_2$ ), different numbers of turns  $N_1$  and  $N_2$ , and opposite currents  $I_1$  and  $-I_2$  ( $I_{1,2} > 0$ ). Here, we define the center of the coils as the origin of the circular coordinate system and the  $z$  axis perpendicular to the coil plane. At a point ( $\rho = 0, \varphi, z = z_0$ ) on the  $z$  axis, the coils produce a magnetic

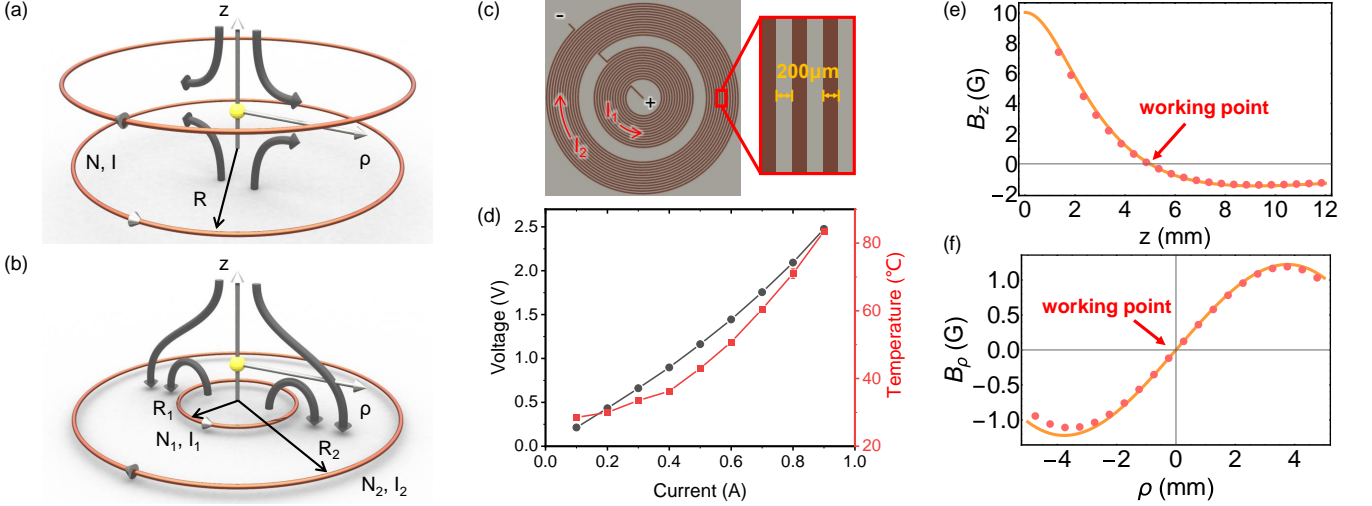


FIG. 1. The planar quadrupole-field coil chip. (a) The conventional anti-Helmholtz coils in a three-dimensional cylindrical geometry. (b) The planar coils. Parameters  $R$ ,  $N$ ,  $I$  are the radii, numbers of turns, and current of each annular coils, respectively. The magnetic field lines are indicated by the grey curves. (c) A practical coil chip consisting of embedded spiraling wires. (d) Steady-state voltage and temperature of the coil chip versus the applied currents. (e) and (f) The magnetic field components along  $z$ - and  $\rho$ -axis.

field intensity  $B = (B_\rho, B_\varphi = 0, B_z)$  as [40]

$$B_z(0, \varphi, z_0) = \frac{\mu_0}{2} \left( \frac{N_1 R_1^2 I_1}{(R_1^2 + z_0^2)^{\frac{3}{2}}} - \frac{N_2 R_2^2 I_2}{(R_2^2 + z_0^2)^{\frac{3}{2}}} \right), \quad (1)$$

$$B_\rho(0, \varphi, z_0) = 0, \quad (2)$$

and the corresponding magnetic field gradients

$$\frac{\partial B_z}{\partial z}(0, \varphi, z_0) = -\frac{3\mu_0 z_0}{2} \left( \frac{N_1 R_1^2 I_1}{(R_1^2 + z_0^2)^{\frac{5}{2}}} - \frac{N_2 R_2^2 I_2}{(R_2^2 + z_0^2)^{\frac{5}{2}}} \right), \quad (3)$$

$$\frac{\partial B_\rho}{\partial \rho}(0, \varphi, z_0) = \frac{3\mu_0 z_0}{4} \left( \frac{N_1 R_1^2 I_1}{(R_1^2 + z_0^2)^{\frac{5}{2}}} - \frac{N_2 R_2^2 I_2}{(R_2^2 + z_0^2)^{\frac{5}{2}}} \right), \quad (4)$$

Due to the cylindrical symmetry,  $\partial B_\rho / \partial \rho = -\frac{1}{2} \partial B_z / \partial z$  on the  $z$ -axis. For simplicity, we first consider the case of balanced currents  $I_1 = I_2 = I$ , which allows the two coils to be connected in series with one current supply. For appropriate  $R_1$  and  $R_2$ , we can adjust  $N_1$  and  $N_2$  to make the field intensities zero at a desired height  $h$ , i.e. at the target MOT working point  $(0, 0, h)$ . As a result, this coplanar coil configuration is able to provide the quadrupole magnetic field for realizing MOT, with a working point above the surface of the coil plane.

A coil chip is constructed based on the printed-circuit-board (PCB) technology, with a chip thickness of  $250 \mu\text{m}$  and an edge length of 3 cm. The coils are made by copper wire printed on a square Rogers ceramic substrate [Fig. 1(c)]. The thickness, width, and spacing of the wire are  $70 \mu\text{m}$ ,  $200 \mu\text{m}$ , and  $200 \mu\text{m}$ , respectively. The inner coil has  $N_1 = 13$  turns,

with a radius ranging from 2.6 mm to 7.8 mm, and the outer coil has  $N_2 = 13$  turns, with a radius ranging from 9.6 mm to 14.8 mm. According to Eq. (1-4), this coil chip has a working point at the height  $h = 5.0 \text{ mm}$ , an axial field gradient of  $\partial B_z / \partial z = 9.8 \text{ G/cm}$  and a radial gradient of  $\partial B_\rho / \partial \rho = -4.9 \text{ G/cm}$  when carrying a current of  $I = 0.9 \text{ A}$ .

Figures 1(e) and (f) show the calculation and measurement results of the axial and radial magnetic fields ( $B_z$  and  $B_\rho$ ). As designed, the coil chip provides an axial gradient of  $9.8 \text{ G/cm}$  and a radial gradient of  $-4.8 \text{ G/cm}$  around the working point with  $h = 5.0 \text{ mm}$ . From the measured field distribution, in a range of about 5 mm along both  $\rho$  and  $z$  directions around the working point, the coil chip can provide the desired magnetic field gradients for the MOT. This provides a sufficiently large volume for confining cold atoms.

Besides the magnetic fields, we also evaluate the performance of the coil chip for practical applications by measuring the steady-state voltage and temperature of the chip versus the current  $I$  [Fig. 1(d)]. The coil chip is placed in an ambient environment underneath the glass cell. At the working current  $I = 0.9 \text{ A}$ , the voltage is measured to be 2.5 V, corresponding to a resistive heating power of 2.2 W. The chip temperature remains at around  $84^\circ \text{C}$ . For application without need for modulation, the coil chip can be replaced by a ring of permanent magnet to remove the power supply and avoid heating issue. In conclusion, the coil chip can provide a stable magnetic field for MOT at a low power setting. This is made possible by the small distances in the planar integration design.

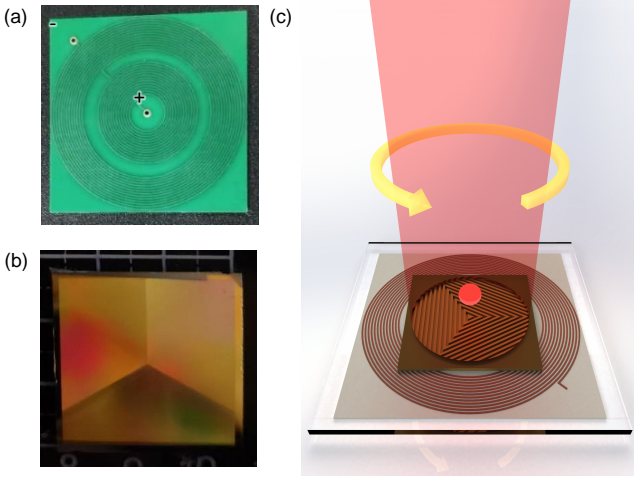


FIG. 2. Experimental apparatus of the planar-integrated MOT. (a) The coil chip. (b) The grating chip. (c) Conceptual sketch of the planar-integrated MOT. The right-handed incident laser beam propagates perpendicular to the chip and produces three first-order diffracted beams.

### III. EXPERIMENTAL PERFORMANCE OF THE PLANAR-INTEGRATED MOT

Figure 2(c) shows a conceptual sketch of the co-integrated MOT based on the combination of a grating chip [Fig. 2(b)] and a coil chip [Fig. 2(a)]. The grating chip consists of three etched gratings on a silicon substrate. Following the pioneering works of the grating MOT [15, 18], the angle between grating periodic directions is  $120^\circ$ , and the grating period and duty cycle are  $1.42 \mu\text{m}$  and  $0.528$ , respectively. The top side of the grating chip is gold-coated to increase diffraction efficiency. The measured diffraction angle is  $33^\circ$  with respect to  $z$ -axis and the diffraction efficiency is  $40\%$ .

In our experiment, the grating chip is mounted underneath and outside the vacuum cell. The coil chip is mounted below the grating chip and aligned so that the two working points of the chips coincide. Two ECDL diode lasers are tuned to the  $780 \text{ nm}$   $^{87}\text{Rb}$  D2 lines. The cooling laser frequency is tuned to the  $^5\text{S}_{1/2}(F=2)$  to  $^5\text{P}_{3/2}(F'=3)$  cycling transition with a detuning  $\sim 12 \text{ MHz}$ , and the repump laser is tuned to the  $^5\text{S}_{1/2}(F=1)$  to  $^5\text{P}_{3/2}(F=2)$  transition. The beams of the two lasers are combined and coupled into a polarization maintaining fiber and delivered to the MOT setup. The incident beam is circularly polarized, has a diameter of  $3.0 \text{ cm}$ , an optical intensity of  $10 \text{ mW/cm}^2$  for the cooling laser and  $1 \text{ mW/cm}^2$  for the repump. Three first-order diffraction beams from the gratings along with the incident beam form a MOT in the presence of a quadrupole magnetic field [see Fig. 2(a)].

By absorption imaging and time-of-flight method, the temperature of the trapped atom cloud is evaluated. Figure 3(a) shows the absorption images of cold atoms following free expansion over a duration  $t$ . Figure 3(b) shows the experimental and fitting results of the atom cloud sizes against  $t$ . The

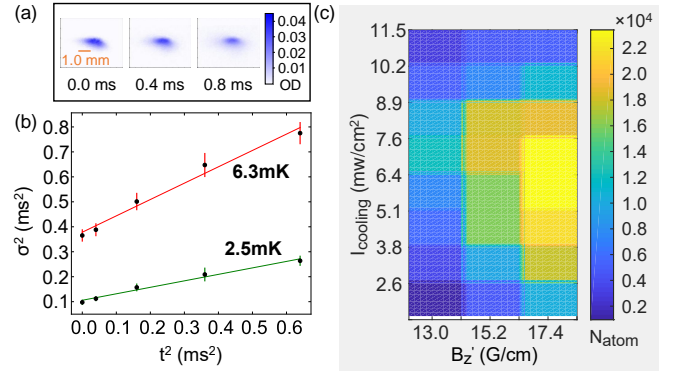


FIG. 3. Experimental performance of planar-integrated MOT. (a) Several absorption images of MOT atoms after free expansion over different times  $t$ . (b) The fitting result of temperature. Two lines are the fits of  $\sigma^2 = \sigma_0^2 + k_B T t^2 / m$  to the data, where  $\sigma$  is the  $1/e$  radii of the cloud,  $k_B$  is the Boltzmann constant,  $T$  is the temperature, and  $m$  is the mass of an  $^{87}\text{Rb}$  atom. (c) Atom number versus axial magnetic field gradient and input cooling laser intensity.

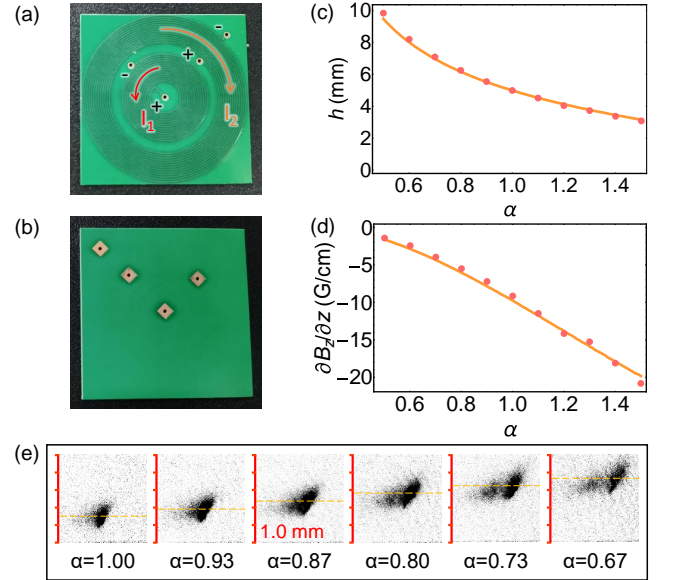


FIG. 4. Experimental performance of adjusting feature without moving. (a), (b) Pictures of two sides of another coil chip design with two independent current supply interfaces. (c) Working point height  $z_0$  versus current ratio  $\alpha$ . (d) Magnetic field gradient at the working point  $B'_z$  versus current ratio  $\alpha$ . (e) Several pictures of MOT status under different  $\alpha$ .

extracted temperature is  $2.5 \text{ mK}$  for the axial direction and  $6.3 \text{ mK}$  for the radial direction. Moreover, we adjust the cooling laser intensity and the magnetic field gradient to examine the system performance, and the results are summarized in Fig. 3(c). At a trapping laser intensity of  $7 \text{ mW/cm}^2$ , the planar-integrated MOT achieves an atom number of  $2 \times 10^4$  and a number density of  $6 \times 10^6 \text{ cm}^{-3}$ .

According to Eq. (1) and Eq. (3), the working point moves vertically when adjusting the ratio of the currents in two pla-

nar spirals  $\alpha = I_2/I_1$ . The orange lines in Figs. 4(c) and (d) show the simulation results of the height of working point  $h$  and the gradient  $\partial B_z/\partial z$ , with  $\alpha$  ranges from 0.5 to 1.5 and  $I_1 = 0.9$  A is fixed. We find that the  $h$  varies from 9.5 mm to 3.2 mm, with the field gradient varying from 1.6 G/cm to 20 G/cm. To verify this result, we modified the coil chip with two sets of printed pads to individually supply the currents for inner and outer coils. The experimental results (red dots) in Figs. 4(c) and (d) fit well with the theoretical predictions. Then, with such a modified coil chip, we realized the adjusting of the atom cloud height from  $\sim 1.5$  mm to  $\sim 3.6$  mm by varying  $\alpha$  from 0.67 to 1.0, as shown by Fig. 4(e). These results indicate a wide tunability of the working point for the planar-integrated MOT with future monolithic integration of the grating and coils.

#### IV. CONCLUSION

In conclusion, we have demonstrated a planar coil configuration to provide a quadrupole magnetic field for realizing a chip-based MOT. Combining two chips, for coil and grating, the planar-integrated MOT is realized for the first time, with significantly reduced volume and weight. This configuration allows more optical access and reduces the power requirements on the current supply and heat dissipation. The planar-integrated MOT also shows excellent compatibility with photonic chips and convenience in alignments, providing an important solution towards a fully integrated cold-atom system for sensors and quantum devices.

#### Acknowledgments

We would like to thank Tianchu Li, Yang Yang and Xiaochi Liu for helpful discussions. The work was supported by the National Key Research and Development Program of China (Grant Nos. 2016YFA0302200 and 2016YFA0301303), the National Natural Science Foundation of China (Grant Nos. 11922411, 11874342, and 41727901), Anhui Initiative in Quantum Information Technologies (Grant No. AHY130200), and the Fundamental Research Funds for the Central Universities (Grant No. WK2470000031). This work was partially carried out at the USTC Center for Micro and Nanoscale Research and Fabrication.

---

\* clzou321@ustc.edu.cn

- [1] H. Zhai, *Reports on Progress in Physics* **78**, 026001 (2015).
- [2] O. Firstenberg, C. S. Adams, and S. Hofferberth, *Journal of Physics B: Atomic, Molecular and Optical Physics* **49**, 152003 (2016), arXiv:1602.06117.
- [3] N. R. Cooper, J. Dalibard, and I. B. Spielman, *Reviews of Modern Physics* **91**, 015005 (2019), arXiv:1803.00249.
- [4] M. Tomza, K. Jachymski, R. Gerritsma, A. Negretti, T. Calarco, Z. Idziaszek, and P. S. Julienne, *Reviews of Modern Physics* **91**, 035001 (2019), arXiv:1708.07832.
- [5] L. Liu, D.-S. Lü, W.-B. Chen, T. Li, Q.-Z. Qu, B. Wang, L. Li, W. Ren, Z.-R. Dong, J.-B. Zhao, W.-B. Xia, X. Zhao, J.-W. Ji, M.-F. Ye, Y.-G. Sun, Y.-Y. Yao, D. Song, Z.-G. Liang, S.-J. Hu, D.-H. Yu, X. Hou, W. Shi, H.-G. Zang, J.-F. Xiang, X.-K. Peng, and Y.-Z. Wang, *Nature Communications* **9**, 2760 (2018).
- [6] J. Grotti, S. Koller, S. Vogt, S. Häfner, U. Sterr, C. Lisdat, H. Denker, C. Voigt, L. Timmen, A. Rolland, F. N. Baynes, H. S. Margolis, M. Zampaolo, P. Thoumany, M. Pizzocaro, B. Rauf, F. Bregolin, A. Tampellini, P. Barbieri, M. Zucco, G. A. Costanzo, C. Clivati, F. Levi, and D. Calonico, *Nature Physics* **14**, 437 (2018), arXiv:1705.04089.
- [7] T. Udem, R. Holzwarth, and T. W. Hänsch, *Nature* **416**, 233 (2002).
- [8] Z.-K. Hu, B.-L. Sun, X.-C. Duan, M.-K. Zhou, L.-L. Chen, S. Zhan, Q.-Z. Zhang, and J. Luo, *Physical Review A* **88**, 043610 (2013).
- [9] E. L. Raab, M. Prentiss, A. Cable, S. Chu, and D. E. Pritchard, *Physical Review Letters* **59**, 2631 (1987).
- [10] K. I. Lee, J. A. Kim, H. R. Noh, and W. Jhe, *Optics Letters* **21**, 1177 (1996).
- [11] M. Vangeleyn, P. F. Griffin, E. Riis, and A. S. Arnold, *Optics Express* **17**, 13601 (2009), arXiv:0905.2897.
- [12] S. Pollock, J. P. Cotter, A. Laliotis, and E. A. Hinds, *Optics Express* **17**, 14109 (2009).
- [13] S. Pollock, J. P. Cotter, A. Laliotis, F. Ramirez-Martinez, and E. A. Hinds, *New Journal of Physics* **13**, 043029 (2011), arXiv:1101.0686.
- [14] M. Vangeleyn, P. F. Griffin, E. Riis, and A. S. Arnold, *Optics Letters* **35**, 3453 (2010), arXiv:1006.4526.
- [15] C. C. Nshii, M. Vangeleyn, J. P. Cotter, P. F. Griffin, E. A. Hinds, C. N. Ironside, P. See, A. G. Sinclair, E. Riis, and A. S. Arnold, *Nature Nanotechnology* **8**, 321 (2013), arXiv:1311.1011.
- [16] J. Lee, J. A. Grover, L. A. Orozco, and S. L. Rolston, *Journal of the Optical Society of America B* **30**, 2869 (2013), arXiv:1309.4732.
- [17] J. P. McGilligan, P. F. Griffin, E. Riis, and A. S. Arnold, *Journal of the Optical Society of America B* **33**, 1271 (2016), arXiv:1601.07431.
- [18] J. P. Cotter, J. P. McGilligan, P. F. Griffin, I. M. Rabey, K. Docherty, E. Riis, A. S. Arnold, and E. A. Hinds, *Applied Physics B* **122**, 172 (2016), arXiv:1601.05548.
- [19] J. Reichel, W. Hänsel, and T. W. Hänsch, *Physical Review Letters* **83**, 3398 (1999).
- [20] J. Denschlag, D. Cassettari, and J. Schmiedmayer, *Physical Review Letters* **82**, 2014 (1999).
- [21] R. Folman, P. Krüger, D. Cassettari, B. Hessmo, T. Maier, and J. Schmiedmayer, *Physical Review Letters* **84**, 4749 (2000).
- [22] J. Rushton, R. Roy, J. Bateman, and M. Himsforth, *New Journal of Physics* **18**, 113020 (2016), arXiv:1607.08662.
- [23] J. Xie, J.-Q. Wang, Z.-B. Wang, X.-X. Hu, X. Guo, R. Niu, J. B. Surya, J.-Z. Zhang, C.-H. Dong, G.-C. Guo, H. X. Tang, and C.-L. Zou, *Opt. Lett.* **44**, 1150 (2019), arXiv:1901.00922.
- [24] X.-X. Hu, J.-Q. Wang, Y.-H. Yang, J. B. Surya, Y.-L. Zhang, X.-B. Xu, M. Li, C.-H. Dong, G.-C. Guo, H. X. Tang, and C.-L. Zou, *Opt. Express* **28**, 11144 (2020).
- [25] J.-Q. Wang, Y.-H. Yang, M. Li, X.-X. Hu, J. B. Surya, X.-B. Xu, C.-H. Dong, G.-C. Guo, H. X. Tang, and C.-L. Zou, *Physical Review Letters* **126**, 133601 (2021), arXiv:2011.10352.
- [26] W. R. McGehee, W. Zhu, D. S. Barker, D. Westly, A. Yulaev, N. Klimov, A. Agrawal, S. Eckel, V. Aksyuk, and J. J. McClelland, *New Journal of Physics* **23**, 013021 (2021).
- [27] M. Kasevich and S. Chu, *Physical Review Letters* **67**, 181 (1991).
- [28] A. Peters, K. Y. Chung, and S. Chu, *Nature* **400**, 849 (1999).



- [29] A. Peters, K. Y. Chung, and S. Chu, *Metrologia* **38**, 25 (2001).
- [30] S.-K. Wang, Y. Zhao, W. Zhuang, T.-C. Li, S.-Q. Wu, J.-Y. Feng, and C.-J. Li, *Metrologia* **55**, 360 (2018).
- [31] L. ESSEN and J. V. L. PARRY, *Nature* **176**, 280 (1955).
- [32] B. de Beauvoir, F. Nez, L. Julien, B. Cagnac, F. Biraben, D. Touahri, L. Hilico, O. Acaf, A. Clairon, and J. J. Zondy, *Physical Review Letters* **78**, 440 (1997).
- [33] P. Laurent, M. Abgrall, C. Jentsch, P. Lemonde, G. Santarelli, A. Clairon, I. Maksimovic, S. Bize, C. Salomon, D. Blonde, J. Vega, O. Grosjean, F. Picard, M. Saccoccio, M. Chaubet, N. Ladiette, L. Guillet, I. Zenone, C. Delaroche, and C. Sirmain, *Applied Physics B* **84**, 683 (2006).
- [34] X. Liu, V. I. Yudin, A. V. Taichenachev, J. Kitching, and E. A. Donley, *Applied Physics Letters* **111**, 224102 (2017).
- [35] X. Liu, E. Ivanov, V. I. Yudin, J. Kitching, and E. A. Donley, *Physical Review Applied* **8**, 054001 (2017).
- [36] L.-M. Duan, M. D. Lukin, J. I. Cirac, and P. Zoller, *Nature* **414**, 413 (2001), [arXiv:0105105 \[quant-ph\]](https://arxiv.org/abs/0105105).
- [37] D.-S. Ding, W. Zhang, Z.-Y. Zhou, S. Shi, G.-Y. Xiang, X.-S. Wang, Y.-K. Jiang, B.-S. Shi, and G.-C. Guo, *Physical Review Letters* **114**, 050502 (2015), [arXiv:1404.0439](https://arxiv.org/abs/1404.0439).
- [38] Y. Wang, J. Li, S. Zhang, K. Su, Y. Zhou, K. Liao, S. Du, H. Yan, and S.-L. Zhu, *Nature Photonics* **13**, 346 (2019), [arXiv:2004.03123](https://arxiv.org/abs/2004.03123).
- [39] R. Wen, C.-L. Zou, X. Zhu, P. Chen, Z. Y. Ou, J. F. Chen, and W. Zhang, *Physical Review Letters* **122**, 253602 (2019), [arXiv:1811.00307](https://arxiv.org/abs/1811.00307).
- [40] T. Bergeman, G. Erez, and H. J. Metcalf, *Physical Review A* **35**, 1535 (1987).